การจำลองเชิงโฟโตอิลาสติกเพื่อการศึกษาปัญหาคานสี่เหลี่ยมที่มีฐานรองรับอย่างง่ายรับแรงเข้มกดที่กึ่งกลางคาน

พิเชษฐ์ พินิจ[1]
มหาวิทยาลัยเทคโนโลยีพระจอมเกล้าธนบุรี แขวงบางมด เขตทุ่งครุ กรุงเทพฯ 10140

บทคัดย่อ

ปัญหาการกระจายความเค้นในคานหน้าตัดสี่เหลี่ยมเป็นปัญหาที่น่าสนใจอย่างยิ่งในทางปฏิบัติเนื่องด้วยโครงสร้างส่วนใหญ่ล้วนประกอบไปด้วยคาน บทความฉบับนี้นำเสนอแบบจำลองทางคณิตศาสตร์ในลักษณะทั่วไปของปัญหาความเค้นระนาบของคานหน้าตัดสี่เหลี่ยมรับแรงเข้มกดที่กึ่งกลางคานตามหลักทฤษฎีของแบร์นูลลี-ออยเลอร์ ทฤษฎีของวิลสัน-สโตกส์ และทฤษฎีดูรัน-การ์วูด และนำเสนอการจำลองเชิงตัวเลขของสนามความเค้นโดยอาศัยหลักการของโฟโตอิลาสติกซิตีเชิงเลข นอกจากนี้บทความยังได้แสดงแผนภาพอื่นใดที่เกี่ยวข้องกับความเค้น ผลจากการคำนวณเชิงตัวเลขและการเปรียบเทียบพบว่า ทฤษฎีดูรัน-การ์วูด แสดงภาพสนามความเค้นและแผนภาพที่เกี่ยวข้องได้ดีกว่าภาพที่ได้จากสองทฤษฎีแรกในด้านของความราบเรียบและความต่อเนื่องของริ้ว อย่างไรก็ดี ทฤษฎีแบร์นูลลี-ออยเลอร์ก็ยังเป็นทฤษฎีที่ให้ความปลอดภัยหรือทฤษฎีเชิงอนุรักษ์สำหรับพื้นที่ส่วนใหญ่ของคานยกเว้นบริเวณจุดที่แรงเข้มกดกระทำ

คำสำคัญ : โฟโตอิลาสติกซิตีเชิงเลข / ริ้ว / ไอโซโครมาติก / ไอโซคลินิก / ไอโซพาชิก / แผนภาพ / คานสี่เหลี่ยมที่มีฐานรองรับอย่างง่าย

[1] *อาจารย์ ภาควิชาครุศาสตร์เครื่องกล คณะครุศาสตร์อุตสาหกรรมและเทคโนโลยี*
E-mail : pichet.pin@kmutt.ac.th

Photoelastic Simulation towards a Study of a Simply Supported Rectangular Beam Carrying a Central Concentrated Force

Pichet Pinit[1]

King Mongkut's University of Technology Thonburi, Bang Mod, Thung Khru, Bangkok, 10140

Abstract

The problem of stress distribution in a rectangular beam is of great practical interest as the beam is used in most structures. This paper presents general mathematical models of a plane-stress problem of a rectangular beam subjected to a concentrated force at its midspan based on three major theories: the Bernoulli-Euler theory, the Wilson-Stokes theory, and the Durant-Garwood theory, and the simulation of the stress field on the basis of the principle of digital photoelasticity. Several relevant maps of stresses are also presented. Comparison of numerical results from these theories reveals that the Durant-Garwood theory gives the stress field being superior to those obtained from the first two theories in the senses of fringes' fineness and continuity. Furthermore, the Bernoulli-Euler theory is shown to be a conservative theory for most regions in the beam except at and near the point of the applied concentrated force.

Keywords : Digital Photoelasticity / Fringe / Isochromatics / Isoclinics / Isopachics / Map / Simply Supported Rectangular Beam

[1] *Lecturer, Department of Mechanical Technology Education, Faculty of Industrial Education and Technology.*
E-mail : pichet.pin@kmutt.ac.th

1. Introduction

Beams with various cross sections are used in several structures such as engines and buildings. Their primary use is to support transverse loads that result a bending and a deflection; these two factors, in turn, have a strong effect on a design of beam in such a way that the bending and deflection lead to suitable shape and stiffness, respectively.

A rectangular beam (Fig. 1) is one of the cross sections being often used; it can be broadly classified into two types: a narrow (long) beam and a deep (short) beam. The difference in the types of the rectangular beam is identified by the half of span-to-depth ratio, l/c , (Fig. 1). If the ratio is just larger than 3 the beam is justified to be the narrow beam; otherwise, it is the deep beam [1]. Correct identification of the types of beam is of importance in that it helps designers simply making a decision of which theories (described next) dominating the design of beam.

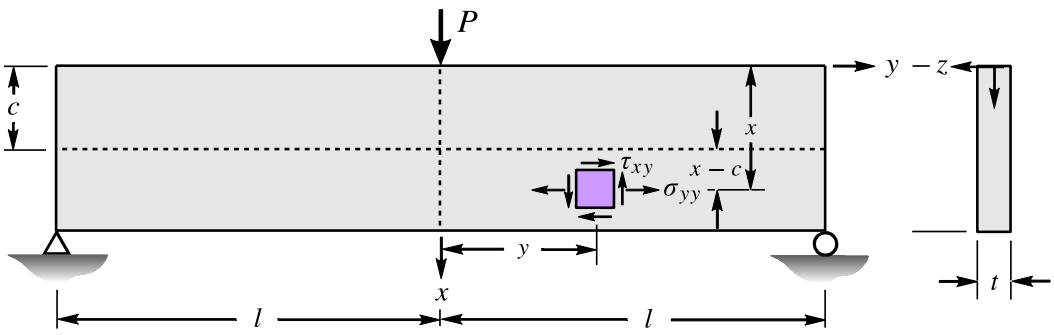

Fig. 1 Geometrical shape and loading condition of the beam used in the Bernoulli-Euler Theory and Wilson-Stokes theory (after Frocht [2]).

Designers use the elementary or technical beam theory (the so-called Bernoulli-Euler theory, BET) to design the beams as the theory is simple and always safe [2]. In view of a stress field, this theory, however, neither furnishes correct stress distribution near points of applied load and the reactive supports nor accounts for a localized effect of concentrated load acting on the beam in spite of the fact that the concentrated load causes high values of stresses. The substantial difference between the results obtained from the photoelastic experiment and the BET exists, especially along the lower edge, and leads to the following aspects [3].

- The actual stress is not linearly proportional to the bending moment, which varies along the beam, as indicated by the BET.
- Near the center of the beam, the values of actual stresses are higher than those predicted by the BET.
- The distribution of the actual stresses shows no discontinuity of slope at the center of beam as shown by the BET.
- The values of actual stresses do not goes to zero as those predicted by the BET; their sign is changed near the reactive supports. This phenomenon is due to a high radial compression produced by the reactive supports.

With the above conclusions, the BET is, therefore, inadequate to give information regarding localized stresses near the active points and supports; nevertheless, the stress field far away

enough from the supports conforms well to the theory. This phenomenon agrees well with the St Venant's principle in that the effect of external force is confined to regions near the points of application of such external force [4]. By the above explanation, we can conclude that the values of stresses predicted by the BET become more unreliable in accordance with a degree of how small the ratio *l/c* is.

To investigate a stress field of the loaded beams and to see how it changes with the ratio *l/c*, this paper presents a simulation of the two-dimensional (2D) stress field, often called a fringe, of the rectangular beam carrying a concentrated force at its midspan based on the principle of digital photoelasticity. Reader can find the detail of the principle of digital photoelasticity in reference [5,6]. Intensity maps of all related stresses are also generated. The paper also provides a numerical comparison of stress results obtained from the BET with other two theories: Wilson-Stokes theory (WST) and Durant-Garwood theory (DGT), for several cross sections of the beam.

A generation code of stress fields and maps is implemented on Visual C++ .NET and can work simply together with or embedded in the program developed elsewhere [7]. The beam can be exploited as a standard photoelastic model in an analysis of stresses as it possesses more complicated stress field than that of a benchmark model-a circular disk model under diametral compression-which makes the beam more suitable for testing other newly developed techniques in the photoelastic analysis [8-10]. The desire to increase the capability of the program [7] in stress analysis lies behind the focus of this paper, which is slanted toward high-end software for the experimental stress analysis.

2. Stresses in Rectangular Beams

Insofar as the literature are reviewed, three explicit systems of 2D stress fields of the rectangular beams based on an analytic derivation are available: the BET, the WST, and the DGT. The BET was derived from the principle of Mechanics or Strength of Materials with several essential assumptions whereas the last two theories were derived on the basis of Theory of Elasticity with rigorous knowledge of mathematics. An in-depth consideration of these theories is addressed as followings.

2.1 Bernoulli-Euler theory

Consider the beam carrying the concentrated force at its center (Fig. 1). Based on the BET, the expressions of stresses in terms of the concentrated force P, the thickness t, and the midspan l are as follow [1];

$$\begin{aligned} \sigma'_{xx} &= 0, \\ \sigma'_{yy} &= \frac{3P}{4tc^3}(l-y)(x-c), \\ \tau'_{xy} &= -\frac{3P}{8tc^3}(2cx-x^2). \end{aligned} \qquad (1)$$

It should be noted that the point of origin of the x-y axis is at the extreme fiber and at the midspan of the beam. Considering the expression of the shear stress τ'_{xy}, we found that it changes its sign when the points in question are on the left side of the x-axis. Additionally, no matter where those points are either above or below the distance c, the sign of the shear stress τ'_{xy} belonging to the points is unaltered as long as those points are on the same side with respect to the x-axis.

2.2 Wilson-Stokes theory

Owing to the concentrated force P acting

on the upper surface of the beam (Fig. 1), we can treat this plane-stress problem as a semi-finite plate subjected to a concentrated force. The expressions of localized stresses in terms of the concentrated force P, the thickness t, and the coordinates x and y are [2]

$$\sigma''_{xx} = -\frac{2P}{\pi t}\frac{x^3}{(x^2+y^2)^2},$$
$$\sigma''_{yy} = -\frac{2P}{\pi t}\frac{xy^2}{(x^2+y^2)^2}, \quad (2)$$
$$\tau''_{xy} = -\frac{2P}{\pi t}\frac{x^2y}{(x^2+y^2)^2}.$$

Combining Eqs. (1) and (2) yields

$$\sigma_{xx} = -\frac{2P}{\pi t}\frac{x^3}{(x^2+y^2)^2},$$
$$\sigma_{yy} = -\frac{2P}{\pi t}\left[\frac{3\pi}{8c}(l-y)(c-x) + \frac{xy^2}{(x^2+y^2)^2}\right], \quad (3)$$
$$\tau_{xy} = -\frac{2P}{\pi t}\left[\frac{3\pi}{16c^3}(2cx-x^2) + \frac{x^2y}{(x^2+y^2)^2}\right].$$

Equation (3) is the well-known WST. Note that the preceding explanation about the change of sign of τ'_{xy} in section 2.1 is also applicable to the shear stress τ_{xy}. Also, this theory is known to hold somewhat as the BET does.

2.2.1 Stress along the section of symmetry: σ_{xx}

Considering now a cross section along the x-axis, we found that the normal stress σ_{xx} must be zero at the bottom surface ($x = 2c$) because there is no applied force acting there. The first expression in Eq. (3) always gives the compressive stress σ_{xx} but its values have to be vanished. If we assume that the correction is of a linear function of x, then, [2]

$$(\sigma_{xx})_{y=0} = -\frac{2P}{\pi tx} + kx. \quad (4)$$

Then, by tedious manipulation with $(\sigma_{xx})_{\substack{x=2c\\y=0}} = 0$, we have $k = P/(2\pi tc^2)$ and

$$(\sigma_{xx})_{y=0} = -\frac{2P}{\pi tx} + \frac{Px}{2\pi tc^2} = \frac{2P}{\pi t}\left(\frac{x}{4c^2} - \frac{1}{x}\right). \quad (5)$$

2.2.2 Stress along the section of symmetry: σ_{yy}

Referring again the cross section along the x-axis, the normal stress σ_{yy} can be modified such that the effect of localized stress is included in it. Considering the second expression of Eq. (3), it is found that [2]

$$(\sigma_{yy})_{y=0} = \frac{3P}{2tc^3}\left(\frac{l}{2} - \frac{c}{\pi}\right)(x-c) + \frac{P}{2\pi ct}. \quad (6)$$

Notice that the first and second expressions on the right side of Eq. (6) accounts for the bending stress and average stress due to the concentrated force, respectively.

2.3 Durant-Garwood theory

Consider Fig. 2 showing the rectangular beam carrying the concentrated force at its midspan. Based on the DGT, let [1]

$$\alpha = \frac{m\pi}{l}, \quad \beta = \alpha c, \quad \xi = \alpha x, \quad \eta = \alpha y, \quad u = \beta - \eta, \quad v = \beta + \eta, \quad (7)$$

and

$$K = \frac{L^2}{4c^3}\left\{p\left[\frac{l_b}{l} - \left(\frac{l_b}{l}\right)^3\right] + q\left[\frac{l_q}{l} - \left(\frac{l_q}{l}\right)^3\right]\right\}, \quad (8)$$

where p and q are the pressure on specific areas, l_p and l_q are the lengths of such areas, respectively, and l_b is the half length of the load-free portion along the lower edge (Fig. 2). Note that the thickness t has already included in the pressure p and q (see Table 1).

Table 1 Values of parameters related to the loading condition used in the DGT

Parameter	Value	Expression
Load-length factor[ล], ***LLF***	0.0250	-
l_q	1.50 mm	$\frac{(LLF)l}{2}$
q	10.0 N/mm^2	$\frac{P}{2tl_q}$
l_p	3.00 mm	$2l_q$
p	5.00 N/mm^2	$\frac{P}{2tl_p}$
l_b	117 mm	-
ρ (epoxy resin)[ว]	1.22×10^3 kg/m^3	-

Note
[ล] This predefined value is equal to $2l_q$.
[ว] This value is taken from Maneschy, C.E., Miyano, Y., Shimbo, M., and Woo, T.C., 1986, "Residual Stress Analysis of an Epoxy Plate Subjected to Rapid Cooling on Both Surfaces", *Experimental Mechanics*, Vol. 26, pp. 306-312.

With the above quantities, the stress components are

$$\sigma_{xx} = Ky + \sum_{m=1}^{\infty}\left\{\left[\frac{h_m \cos\xi}{(\sinh^2 2\beta - 4\beta^2)}\right][\sinh 2\beta(u\cosh v - \sinh v) - 2\beta(v\cosh u - \sinh u)]\right\} + \sum_{m=1}^{\infty}\left\{\left[\frac{a_m \cos\xi}{(\sinh^2 2\beta - 4\beta^2)}\right][\sinh 2\beta(v\cosh u - \sinh u) - 2\beta(u\cosh v - \sinh v)]\right\}, \quad (9)$$

$$\sigma_{yy} = \frac{1}{2l}(ql_q + pl_p) - \rho g y - \sum_{m=1}^{\infty}\left\{\left[\frac{h_m \cos\xi}{(\sinh^2 2\beta - 4\beta^2)}\right](u\sinh 2\beta\cosh v - 2\beta v\cosh u + \sinh 2\beta\sinh v - 2\beta\sinh u)\right\} - \sum_{m=1}^{\infty}\left\{\left[\frac{a_m \cos\xi}{(\sinh^2 2\beta - 4\beta^2)}\right](v\sinh 2\beta\cosh u - 2\beta u\cosh v + \sinh 2\beta\sinh u - 2\beta\sinh v)\right\}, \quad (10)$$

and

$$\tau_{xy} = \sum_{m=1}^{\infty}\left\{\left[\frac{h_m \sin\xi}{(\sinh^2 2\beta - 4\beta^2)}\right](u\sinh 2\beta\sinh v + 2\beta v\sinh u)\right\} - \sum_{m=1}^{\infty}\left\{\left[\frac{a_m \sin\xi}{(\sinh^2 2\beta - 4\beta^2)}\right](v\sinh 2\beta\sinh u + 2\beta u\sinh v)\right\}. \quad (11)$$

where $a_m = \frac{2q \sin \alpha l_q}{m\pi}$, $h_m = -\frac{2p \sin \alpha l_b}{m\pi}$, ρ is a desity of materials used to fabricate the beam, and g is the gravitational acceleration. Note that the BET and the WST do not account for the beams' materials. The term $\rho g y$ is a compressive stress due to the weight of the beam.

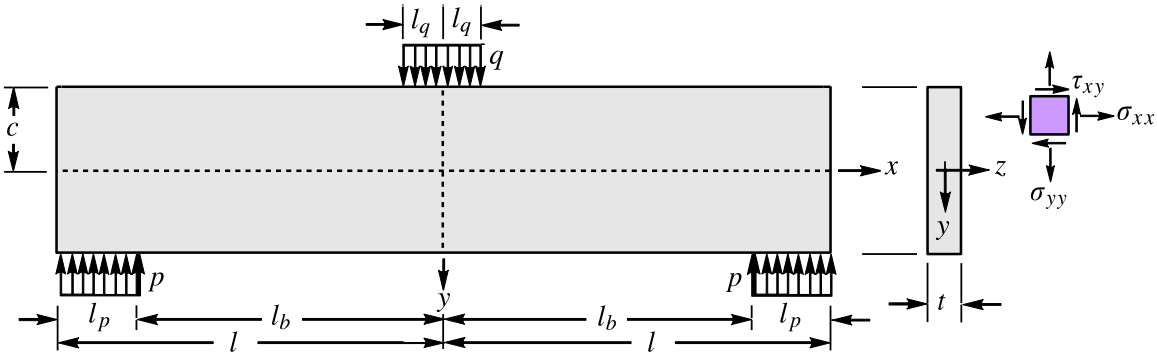

Fig. 2 Geometrical shape and loading condition of the beam used in the Durant-Garwood theory (after Sadd and Hendry [1]).

3. Computer-based Generation of Stress Fringes and Maps

Before we make any further consideration, an explanation about the difference between the fringe and map must be made. In digital photoelasticity, the fringe refers to an image representing the field of wavy-colored bands by which the color and shape of the field change due to the values of the parameters in the governing intensity equations [5]. These parameters, in turn, directly pertain to the physical quantities needed to be interpreted. On the other hand, the map is an image representing the field of a non-wavy-colored band generated from the values of one interested parameter such as σ_{xx}, σ_{yy}, τ_{xy}, and so on.

3.1 Stress Fringes and Maps

In this study, several fringes as well as maps of relevant parameters involving in the photoelastic analysis are considered. They are as follows.

3.1.1 Maps of individual stress

Several sets of stress components associated with their theories are available in section 2, i.e., σ_{xx}, σ_{yy}, and τ_{xy}, each of which can be plotted individually. Further, the individual principal stress, σ_1 and σ_2, maximum shear stress, $\tau_{\max}$, and von-Mises stress, σ_{vonMises}, can also be computed from those stress components using the following well-known equations.

$$\sigma_{1,2} = \frac{\sigma_{xx} + \sigma_{yy}}{2} \pm \frac{1}{2}\sqrt{(\sigma_{xx} - \sigma_{yy})^2 + 4\tau_{xy}^2}, \quad \textbf{(12)}$$

$$\tau_{\max} = \frac{1}{2}\sqrt{(\sigma_{xx} - \sigma_{yy})^2 + 4\tau_{xy}^2} = \frac{1}{2}(\sigma_1 - \sigma_2), \quad \textbf{(13)}$$

$$\begin{aligned}\sigma_{\text{vonMises}} &= \sqrt{(\sigma_{xx}^2 - \sigma_{xx}\sigma_{yy} + \sigma_{yy}^2 + 3\tau_{xy}^2)} \\ &= \sqrt{(\sigma_1^2 - \sigma_1\sigma_2 + \sigma_2^2)}.\end{aligned} \quad \textbf{(14)}$$

3.1.2 Maps of total isochromatic fringe order and wrapped isochromatics

The isochromatics (fringe order), $N_{\text{isochromatic}}$, can be obtained using the equation below for each particular wavelength i; that is (see Eq.(13)),

$$N_{\text{isochromatic},i} = \frac{t}{f_{\sigma,i}}\sqrt{(\sigma_{xx}-\sigma_{yy})^2+4\tau_{xy}^2} = \frac{t}{f_{\sigma,i}}(\sigma_1-\sigma_2), \quad (15)$$

where $f_{\sigma,i}$ is the so-called material fringe values and determined by a calibration method for such particular wavelength. If a color image is of interest, i represents each color plane in ordinary color images, i.e. red (R), green (G), and blue (B). Since the spectrum of the visible or white light covers a wide range of wavelength, the exact values of R, G, and B wavelengths are indeterminate. However, the closet values of representing the white light are given elsewhere in many standard textbooks of digital image processing (DIP).

The wrapped isochromatics map is available with the simple operation according to the following relation.

$$N^{\text{w}}_{\text{isochromatic},i} = N_{\text{isochromatic},i} - \text{INT}\left[N_{\text{isochromatic},i}\right], \quad (16)$$

where $N^{\text{w}}_{\text{isochroma},i}$ represents the wrapped values of the isochromatics as indicated by the superscript text 'w' and the function INT[$\mathbb{R}$] gives a nearest integer of any real number $\mathbb{R}$.

3.1.3 Map of total isopachic fringe order and wrapped isopachics

We can generate the map of isopachic fringe order, $N_{\text{isopachic}}$, by the same way as that of the isochromatic fringe order (see Eq. 1.5 of the total isochromatic fringe order); that is,

$$N_{\text{isopachic},i} = \frac{t}{f_{\sigma,i}}(\sigma_1+\sigma_2) \quad \text{or} \quad N_{\text{isopachic},i} = \frac{t}{f_{\sigma,i}}(\sigma_{xx}+\sigma_{yy}). \quad (17)$$

The sum of principal stresses satisfies the well-known Laplace's equation, $\nabla^2(\sigma_1+\sigma_2)=0$. This equation can be solved using the standard numerical method of finite difference but solving the Laplace's equation is beyond the scope of the present work.

For the wrapped isopachics map, it can be retrieved with the simple operation as shown in Eq. (16); that is,

$$N^{\text{w}}_{\text{isopachic},i} = N_{\text{isopachhic},i} - \text{INT}\left[N_{\text{isopachic},i}\right], \quad (18)$$

where $N^{\text{w}}_{\text{isochroma},i}$ represents the wrapped values of the isopachics and the superscript text conveys the same meaning as in Eq. (16).

3.1.4 Isochromatic, isoclinic, and photoelastic fringes

Based on the plane polariscope, the photoelastic fringe contains both isochromatic and isoclinic fringes. To plot the isochromatic fringe, it is just that we cancel out the isoclinic term in the governing intensity equation. It should be noted that, in practice, we cannot obtain the isochromatic fringe by just only considering the isochromatic term since the isochromatic and isoclinic fringes are combined by nature except that we exploit the circular polariscope.

We can retrieve the map of isoclinics using the well-known following equation.

$$\phi = \frac{1}{2}\arctan\left[\frac{2\tau_{xy}}{(\sigma_{xx}-\sigma_{yy})}\right] \quad \text{or} \quad \phi = \frac{1}{2}\arctan\left[\frac{2\tau_{xy}}{(\sigma_{yy}-\sigma_{xx})}\right]. \quad (19)$$

Equation (19) enables two values of ϕ, each of which corresponds to the directions of the principal stresses σ_1 and σ_2. The way to correctly match those isoclinic values and the principal stresses is described elsewhere [12]. Plotting the isoclinic fringe is similar to plotting the isochromatic fringe but with the exclusion of the isochromatic term in the governing intensity equation. Note that the left expression in Eq. (19) is applicable to the DGT whereas the right one is for the first two theories.

The procedure for the generation of photoelastic fringes is mentioned elsewhere [11] but, for clarity, it is briefly addressed here as follows: (1) Determine the isochromatics and the isoclinics by use of Eqs. (15) and (19), respectively; and (2) Input the values computed in (1) in the governing intensity equation [7] to plot the photoelastic fringes.

3.1.5 Isoclinic map

With Eq. (19), we get the isoclinic values at every point (x, y) in the region of interest (ROI). These values are used to plot the map, directly, instead of using the governing intensity equation as in the plot of isoclinic fringe.

3.2 Graphical plot of fringes and maps

For data visualization, the values of those interested parameters are codified to the corresponding images by the following equation.

$$g(x, y) = \mathrm{INT}\left[255\left(\frac{\upsilon - \upsilon_{\min}}{\upsilon_{\max} - \upsilon_{\min}}\right)\right], \qquad \textbf{(20)}$$

where $g\ (x, y)$ is a gray value of a pixel at the position (x, y). The function $\mathrm{INT}[\mathbb{R}]$ gives a nearest integer of any real number $\mathbb{R}$. The number of 255 is a maximum value of digitization and υ, $\upsilon_{\max}$, and $\upsilon_{\min}$ are, respectively, the to-be-codified, maximum, and minimum values of parameters interested.

4. Conditions for Fringe Generation

For the generation of fringes and maps, the material stress fringe values for three RGB wavelengths already reported are used [8]: $f_{\sigma,\mathrm{R}} = 11.19$, $f_{\sigma,\mathrm{G}} = 10.01$, and $f_{\sigma,\mathrm{B}} = 7.99$, $\mathrm{N\cdot mm^{-1}\cdot fringe^{-1}}$. These values, however, can be obtained for any other wavelength using the standard calibration method [13]. Two ratios of l/c = 2.00 and l/c = 4.00 with l = 120.00 mm. are used and they were chosen in order that we can easily investigate the change of stress fields of the beams as addressed in ref. [1]. The magnitude of load P applied at the midspan is of 300.00 N. Table 1 lists values of those parameters pertaining to the DGT.

5. Program Implementation

The generation code is implemented in Visual C++ .NET as a stand-alone module according to the Object-Oriented Programming (OOP) concept. It gives several types of fringes and maps according to information previously described, and is embedded in the program already written [7].

Considering the DGT, we see that the stress components are expressed in the form of summation with an index m running from 1 to ∞. Since it is impossible for the computer to sum the stress values for such value of m, a predefined value must be used. The only condition used to determine the m value is the smoothness of the fringe fields. It was empirically found that the m value of 100 provided sufficient smooth fringes and maps. The m value is of user-dependent; the higher the m value is, the slower the fringe or map is generated.

In Fig. 3 is shown the data-inputting dialog for several parameters needed for the simulation such as beam theories, beam properties, magnitude of applied load, fringe or map types, and so on. Table 2 lists all available types of fringe and map. The

user can select one of the theories at a time. Other parameters can also be changed by inputting a proper value into the edit box nearby. The options of '-45 to +45 deg' and '-90 to +90 deg' are only available as soon as the user select 'Isoclinic map' in the list (Fig. 3b). The difference of these two options is that the '-45 to +45 deg' option provides the directions of the principal stress between -45° to +45° as theoretically computed using Eq. (19) whereas the '-90 to +90 deg' option give the physical range that is unobtainable with Eq. (19) but with the phase unwrapping process. Detail about this difference has been described elsewhere [12]. Moreover, the 'Summation' field is activated once the 'Durant-Garwood' option is checked. The 'Max fringe' field is only turned on when the 'Total isochromatic fringe order map' in the list is selected. The 'Default' button brings back every change made by the user to the original setting (Fig. 3a). It should be noted that the 'Angle' field is the isoclinic value supplied by the user to be used later in the plot of 'Photoelastic fringe' and 'Isoclinic fringe' as it is needed in the governing intensity equation.

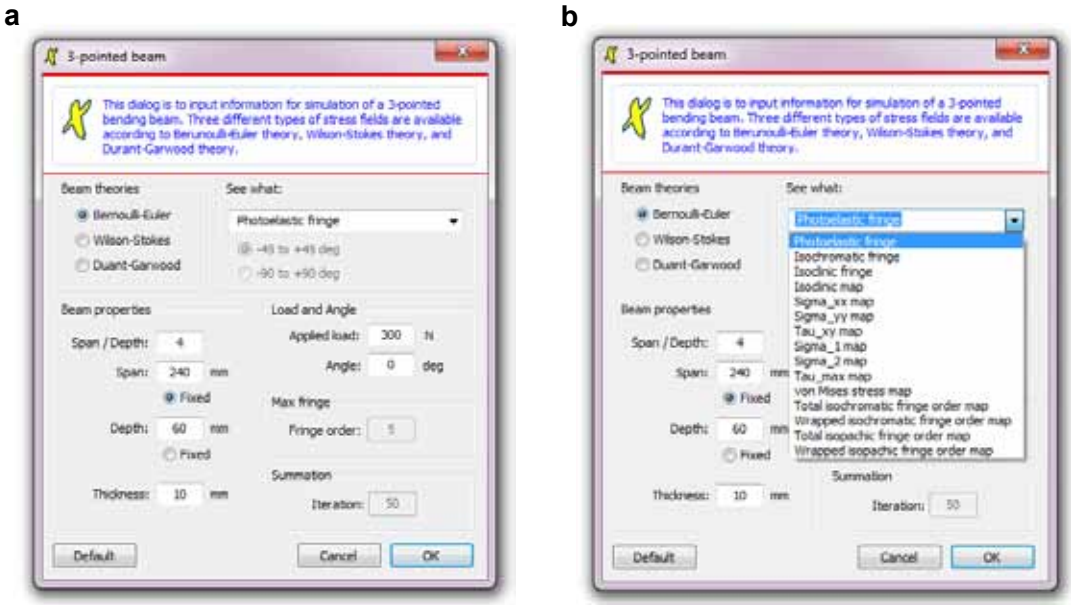

Fig. 3 Data-inputting dialog with several parameters required for the fringe and map simulation: (a) interface once opened and (b) interface showing several types of fringe and map.

Table 2 Stress fields with their available fringes and maps

Stress field	Fringe	Map
σ_{xx}	-	✓
σ_{yy}	-	✓
τ_{xy}	-	✓
σ_1	-	✓
σ_2	-	✓
$(\sigma_1 - \sigma_2)$	-	✓
$(\sigma_1 + \sigma_2)$	-	✓
$\tau_{\max}$	-	✓
σ_{vonMises}	-	✓
isochromatics, $N_{\text{isochromatic}}$	✓	✓
isoclinics, ϕ	✓	✓
isopachics, $N_{\text{isopachic}}$	✓	✓
photoelastic	✓	-

6. Results and Discussion

Fig. 4, 5, and 6 respectively show sets of photoelastic fringes, isochromatics fringes, and isoclinic maps generated using those theories with different ratios of *l/c*. In Fig. 6 is shown both the wrapped (-45° to +45°) and unwrapped (-90° to +90°) isoclinic values.

One sees that the simulated photoelastic fringes based on the use of the BET show considerable difference from those fringes obtained from the other two theories. The effect of the concentrated force (a high fringe density) at the upper edge of the beam is obvious in Figs. 4b and 4c, and Figs. 5b and 5c with small difference at the fringe loops (colored ellipses near the load application point) whereas such effect does not exist in Figs. 4a and 5a. Further consideration of Figs. 4a and 5a reveals that the fringes are horizontally symmetric. It is seen in Fig. 5 that the stress level at the lower edge (region) computed from the BET and the WST is higher than that computed from the DGT for both *l/c* ratios. This difference is clear in that the brightness of color of such region in Fig. 5c is less than that in Fig. 5b. Considering Fig. 5 (left side) again reveals that the simulated fringes obtained from the DGT provides a realistic perspective in having the proper compressive-force path; that is, the applied load is transferred to the reactive supports along the shortest path [13]. This force path is clearly seen in Fig. 5c as the regions of high stress value that connect the load application point and the reactive points and it can help the design of the reinforced concrete (RC) deep beam based on the compressive strut and tension tie model [4,14]. Note that the tension ties can be applied along both the lower edge and the direction perpendicular to the compressive-force path to prevent a crack in concrete.

Fig. 7 displays sets of maps of stress components, σ_{xx}, σ_{xy}, and τ_{xy} generated using those three theories with the ratio *l/c* = 4.00. Note that those

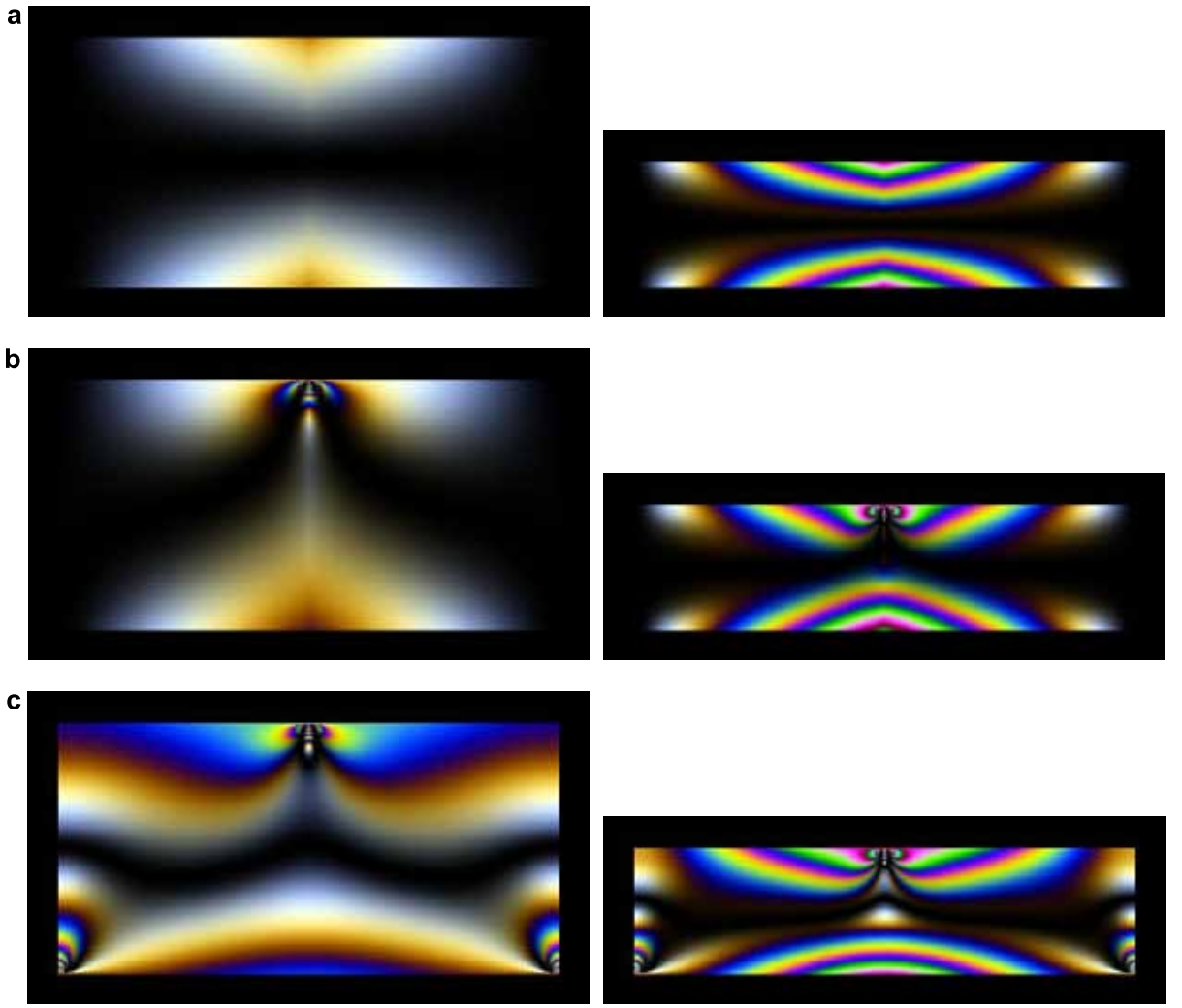

Fig. 4 Photoelastic fringes simulated with the ratios l/c = 2.00 (left) and l/c = 4.00 (right), and ϕ = 45° exploiting (a) the Bernoulli-Euler Theory, (b) the Wilson-Stokes theory, and (c) the Durant-Garwood theory.

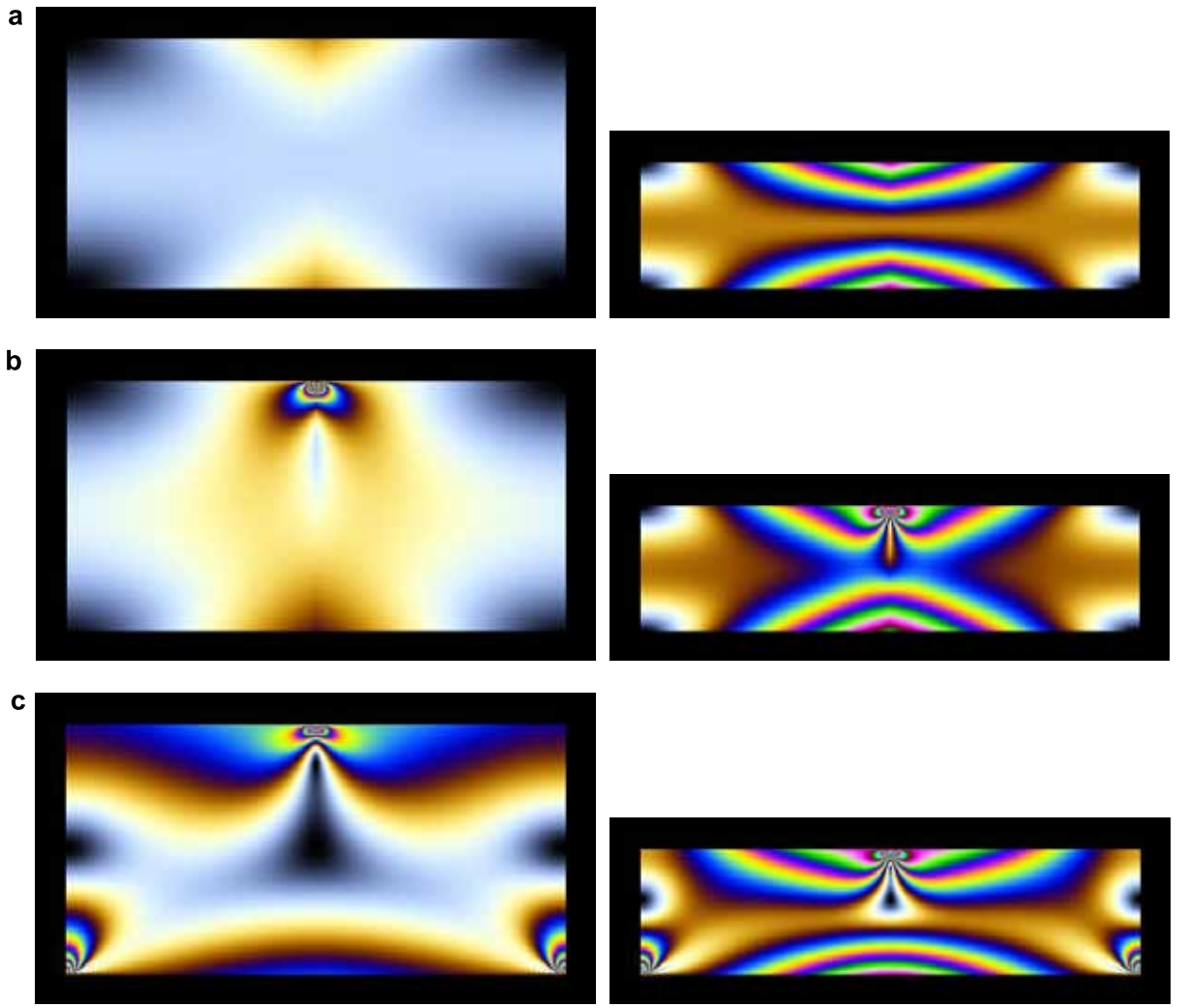

Fig. 5 Isochromatic fringes simulated with the ratios l/c = 2.00 (left) and l/c = 4.00 (right) exploiting (a) the Bernoulli-Euler Theory, (b) the Wilson-Stokes theory, and (c) the Durant-Garwood theory.

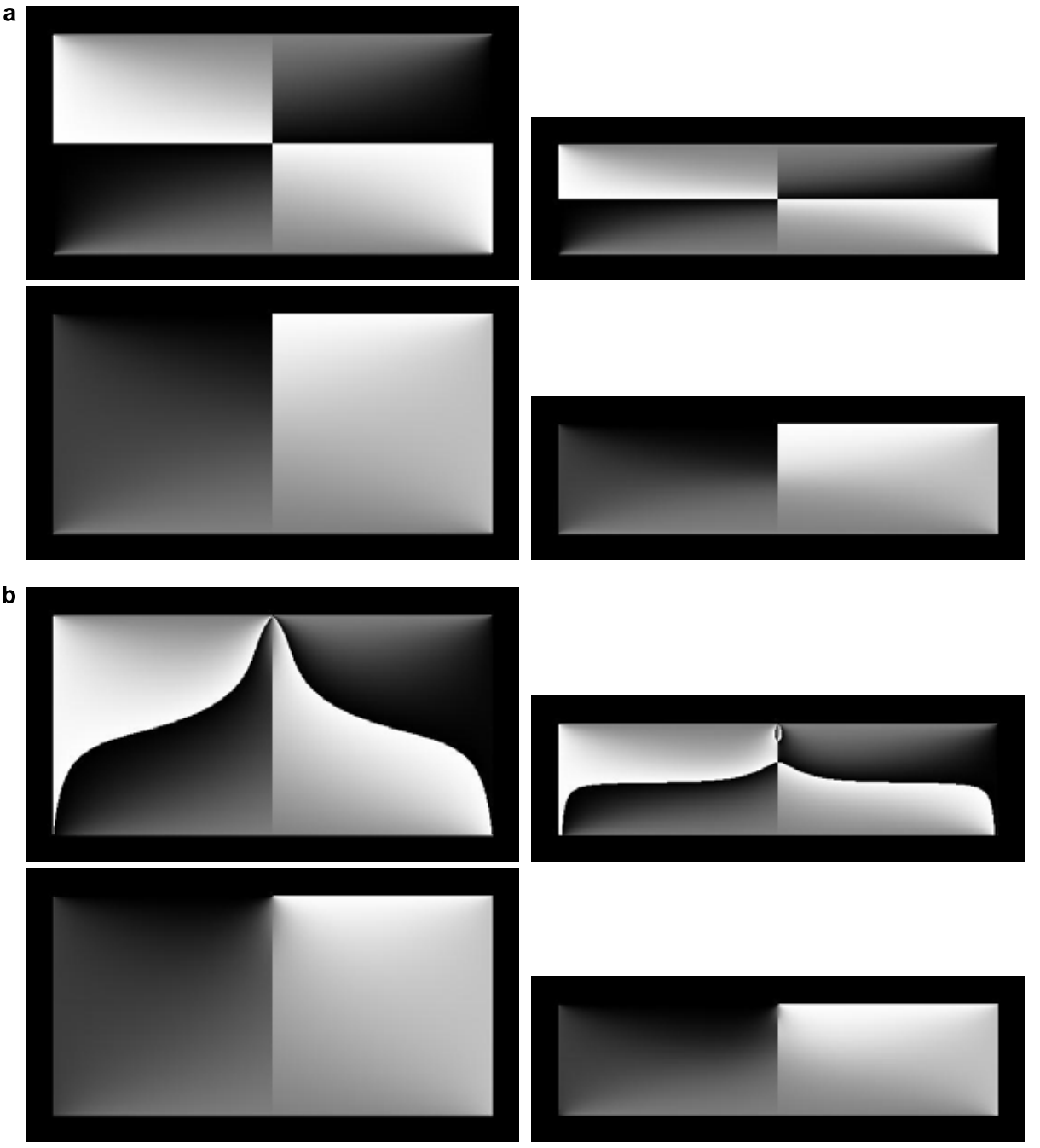
a
b

c

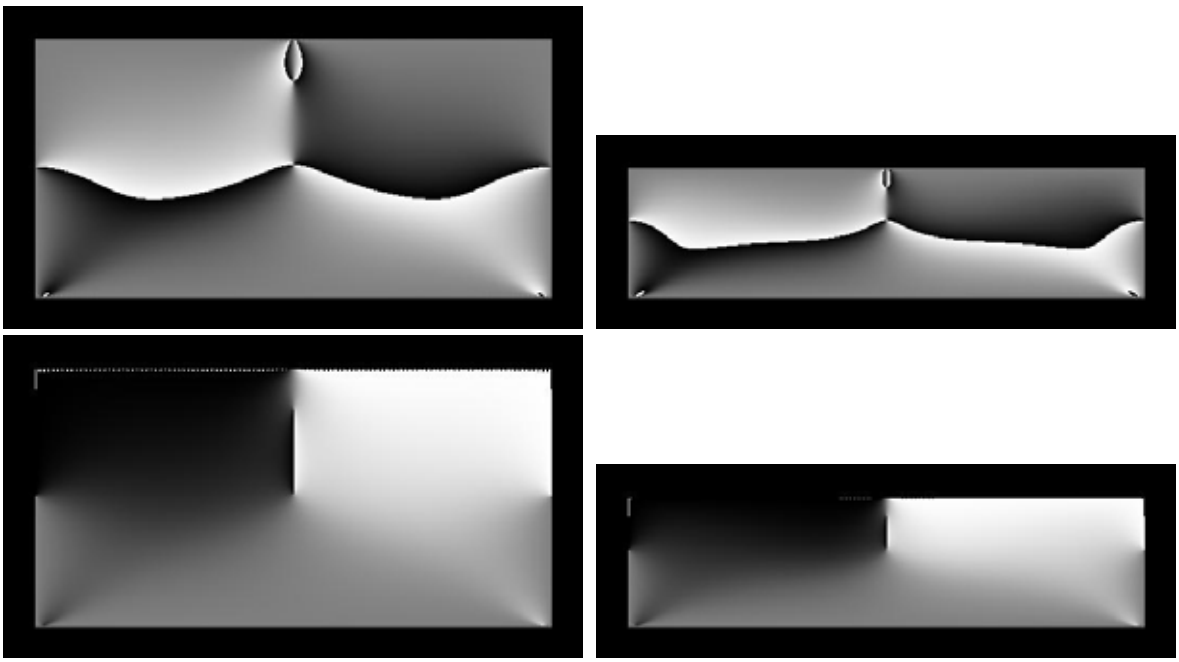

Fig. 6 Isoclinic fringes simulated with the ratios *l/c* = 2.00 (left) and *l/c* = 4.00 (right) exploiting (a) the Bernoulli-Euler Theory, (b) the Wilson-Stokes theory, and (c) the Durant-Garwood theory. In each theory, the upper and lower maps refer to the isoclinic values in the ranges -45° to +45° and -90° to +90°, respectively.

maps generated with the ratio of l/c = 2.00 are not shown here owing to the similarity of fringe patterns. Further, the fringe intensity of the same stress component is slightly different due to the use of Eq. (20) with different values of υ_{max} and υ_{min} except for the shear stress τ_{xy}. For the normal stress σ_{xy}, we can see the effect of the concentrated force in the maps generated using the WST and the DGT (Figs. 7b and 7c). Although the maps of the shear stress τ_{xy} are different, their sign is the same; this can be seen by considering the white and black colors near the application point and the reactive supports.

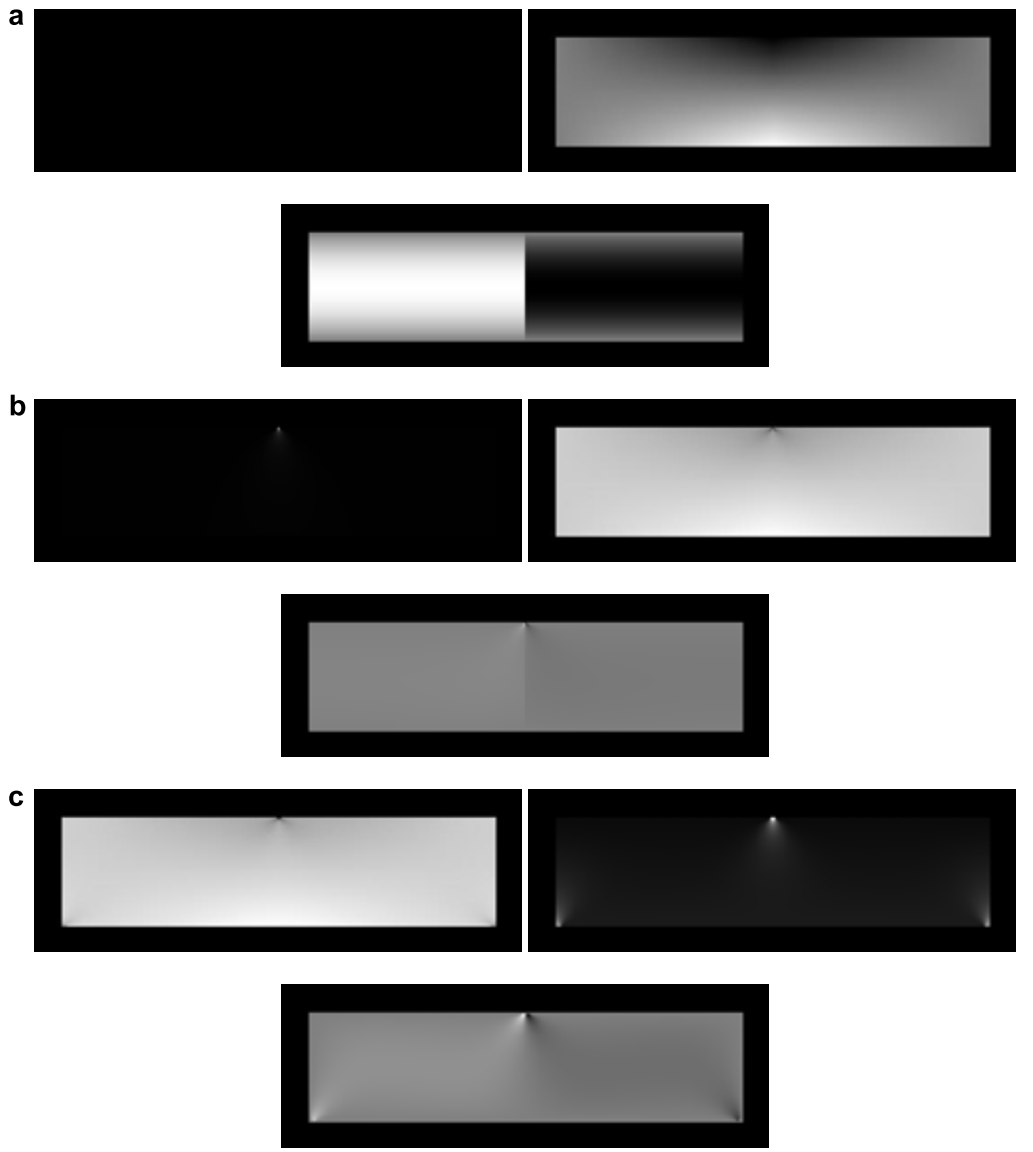

Fig. 7 Maps of σ_{xx}, σ_{yy}, and τ_{xy} generated with the ratio l/c = 4.00 exploiting (a) the Bernoulli-Euler Theory, (b) the Wilson-Stokes theory, and (c) the Durant-Garwood theory. Read horizontally and vertically.

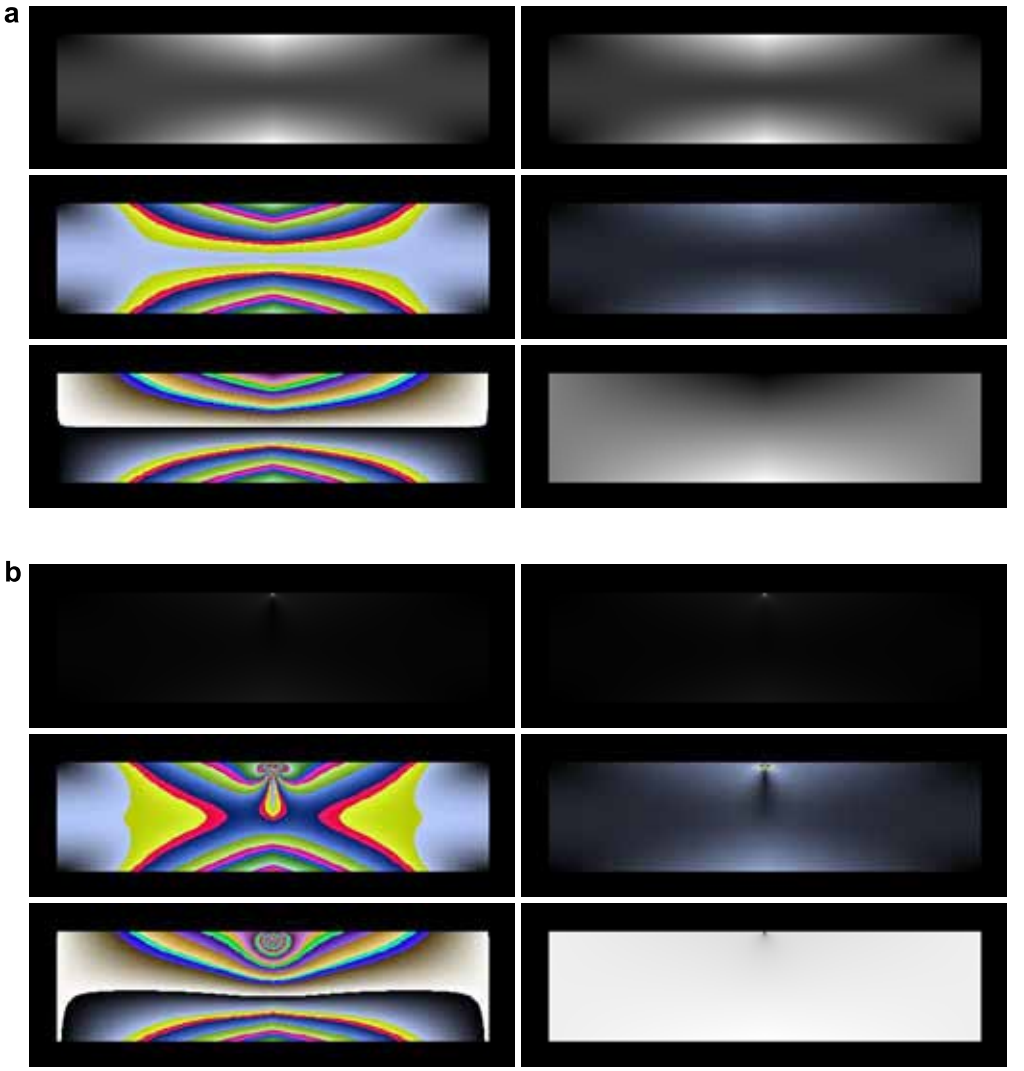
a
b

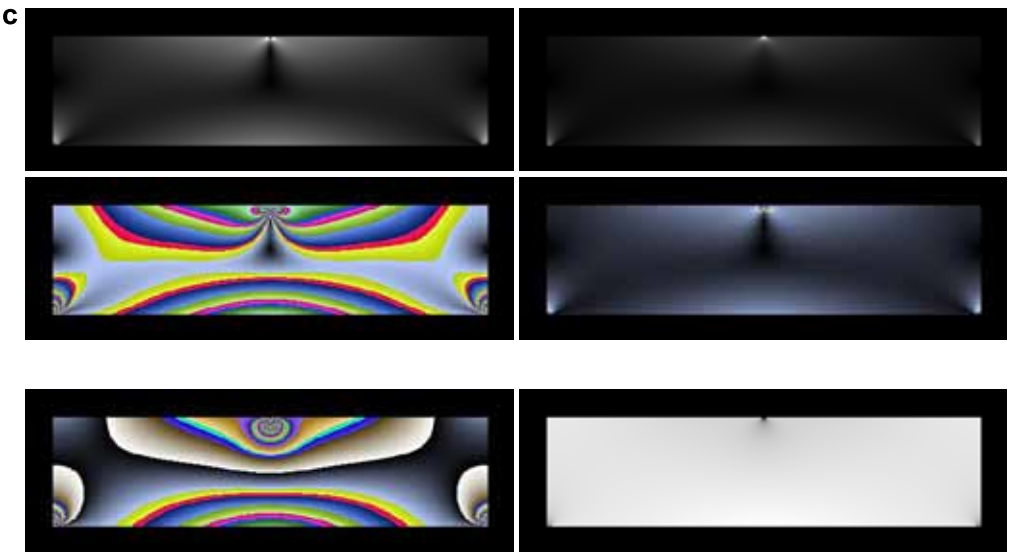

Fig. 8 Maps of τ_{max}, $\sigma_{vonMises}$, $N^{w}_{isochromatic}$, $N_{isochromatic}$, $N^{w}_{isopachic}$, and $N_{isopachic}$ generated with the ratio $l/c = 4.00$ exploiting (a) the Bernoulli-Euler Theory, (b) the Wilson-Stokes theory, and (c) the Durant-Garwood theory. Read horizontally and vertically.

In Fig. 8 are shown sets of maps of τ_{max}, $\sigma_{vonMises}$, $N^{w}_{isochroma}$, $N_{isochroma}$, $N^{w}_{isopachic}$, and $N_{isopachic}$ generated using those three theories with the ratio l/c = 4. It is also noted that those maps generated with the ratio of l/c = 2.00 are not shown here owing to the similarity of fringe patterns as mentioned in previous paragraph. One see that the maps of τ_{max} and $\sigma_{vonMises}$ (each top row) are individually almost the same. These maps are important in the failure theories: Maximum Shear Stress Theory (MSST) and Distortion Energy Theory (DET) (or Octahedral Shear Stress Theory). It is well known that the MSST is more conservative than the DET [15]. This is consistent with the design principle in that the bigger the size of a designed member, the better the resistance of that member to the failure. In other words, the member size designed using the MSST is always bigger than that designed based on the DET. This principle is true with the cost of a design cost. The conservative sense is clearly seen in that the map of τ_{max} looks always brighter than the map of $\sigma_{vonMises}$ for the same magnitude of the applied concentrated force.

The other three sets of four images show sequentially the maps of wrapped and unwrapped isochromatics, and wrapped and unwrapped isopachics. The maps of wrapped and unwrapped isochromatics simulated using the WST and the DGT look similar; however, the wrapped one that generated from the BET shows no effect of concentrated force. The effect of concentrated force appears both at the load application point and at the reactive supports in the maps obtained from the DGT which give more reality than the first two theories. The foregoing description is also applicable for the maps of wrapped and unwrapped isopachics.

It is of practical interest to compare the bending stresses obtained from those theories. In Fig. 9 are shown curves of σ_{yy} (σ_{xx} for the DET) where the horizontal axis shows the stress value whereas the vertical axis show the points of interest starting from the top edge down to the lower edge of the beam along the x-axis (see also Fig. 1). Consider the curves of bending stress for the ratio of l/c = 2.00 (Fig. 9a). The stress curves of the BET and WST show linear distribution with a discrepancy near the load application point in that the WST provides much higher compressive normal stress. This linear distribution also occurs for the case of the Modified WST and DGT. We can also see that the WST and DGT show a similar trend toward greater compressive normal stress but the DGT provides a smooth curve near the load application point. Information just mentioned is also true for curves shown in Figs. 9b, 9c, and 9d (l/c = 3.00, l/c = 4.00, and l/c = 5.00, respectively). However, the stress curves of the DGT shows a nonlinear trend and considerable deviations from other theories with increasing the ratio of l/c. Also, the effect of the concentrated force causes a downward movement of a sharp-curved portion near the load application point. It is seen that the stress curves of the Modified WST and DGT agree well for every ratio of l/c in Fig. 9. Note that the Modified WST is available only along the x-axis.

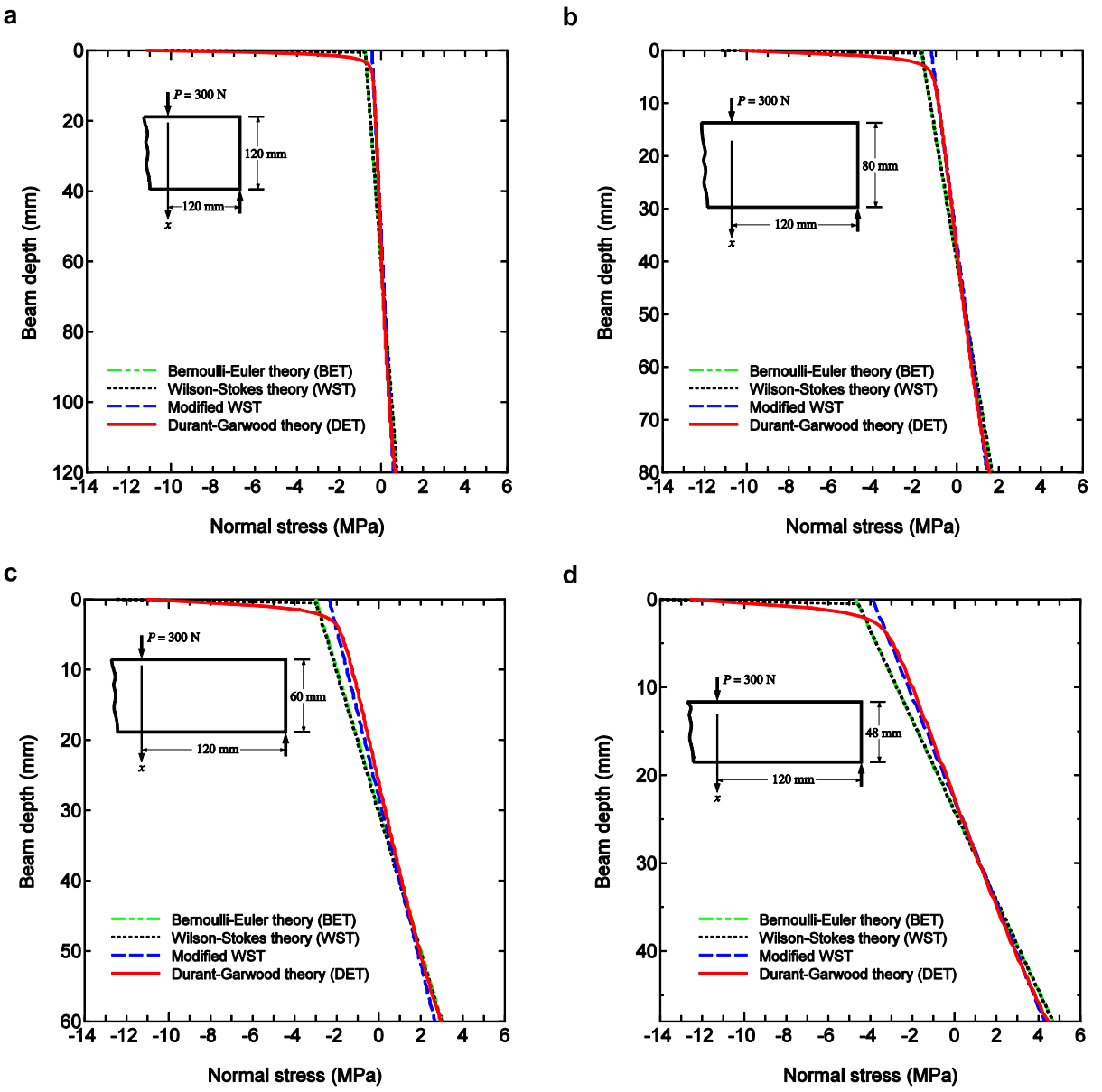

Fig. 9 Curves of bending stress σ_{yy} (σ_{xx} for the Durant-Garwood theory) obtained with the ratios of (a) l/c = 2.00, (b) l/c = 3.00, (c) l/c = 4.00, and (d) l/c = 5.00 along the x-axis under the load application point. Data from the Bernoulli-Euler Theory is represented by the green two-dot-dashed line, the Wilson-Stokes theory and its modified version (use of Eq. 6) by the black dotted line and blue dashed line, respectively, and the Durant-Garwood theory by the red solid line.

7. Conclusion

Digitally photoelastic simulation of the stress and/or fringe field of the rectangular beam is proposed through the program module. Three general mathematical models of the beam theories are discussed. It has been shown that the close agreement of the stress curves indicates the accuracy of numerical results for the small ratio of l/c: $l/c \leqslant 3$. However, the considerable deviation of these numerical resultsappears when $l/c \geqslant 4$, especially the compressed part of the beam. We have seen that the numerical results predicted by the BET are always greater than those from the WST and the DGT, which is consistent to the conclusion of Frocht [2]; however, the only exception is at and near the load application point.

It seems that there is a disagreement between the conclusions mentioned by Frocht [2] and by Kuske and Robertson [3]. That is, Frocht states that the BET is always safe or conservative whereas Kuske and Robertson observe that near the center of the beam, the values of actual stresses are higher than those predicted by the BET (see third paragraph of section 1). This disagreement is due to the fact that the BET requires the external force to be distributed parabolically over the cross section as the internal shear force [3]. The way to demonstrate such parabolic distribution is to make the beam having small transverse wings with reasonable width at the load application point and the reactive supports, and to have the external load applying at both ends of the central wing. With information just mentioned, the validity of the BET, strongly depends on the loading condition and the shape of beam.

To make the program module more practicable in studying the beam problem, the following aspects should be addressed: (1) in Table 1, the Load-length factor, *LLF*, is judiciously predefined for the DGT and it causes l_q = 1.5 which is only equal to 1.25% of the half span l. So, increasing the length l_q would be beneficial for the study of the stress and/or fringe field for the condition of distributed load acting on the beam, and (2) it is only that the DGT accounts for the stress due to the weight of beam; therefore, the simulation of stress and/or fringe field with various values of material density would be of interest. Attention must be paid, however, when we use different materials because the parameter f_σ is dependent of materials and the wavelength used in the calibration.

8. Acknowledgement

The Faculty of Industrial Education and Technology (FIET) is fully acknowledged for the permission of using the Microsoft Visual C++ .NET 2008 (a copyright of academic edition) to program all of the generation code.

9. References

1. Sadd, S. and Hendry, A.W., 1961, "Stresses in a Deep Beam with a Central Concentrated Load", *Experimental Mechanics*, Vol. 1, pp. 192-198.

2. Frocht, M.M., 1948, *Photoelasticity*, Vol. 2, John Willey & Sons, New York.

3. Kuske, A. and Robertson, G., 1974, *Photo elastic Stress Analysis*, John Willey & Sons, London.

4. Nagarajan, P. and Pillai, M., 2008, "Development of Strut and Tie Models for Simply Supported Deep Beams using Topology Optimization", *Songklanakarin Journal of Science and Technology*, Vol. 30, pp. 641-647.

5. Ramesh, K., 2000, *Digital Photoelasticity: Advanced Techniques and Applications*, Springer, Germany.

6. Pinit, P., 2009, "Overview of Photoelasticity and Digital Photoelasticity", *KKU Engineering Journal*, Vol. 36, pp. 195-203. (In Thai)

7. Pinit, P., 2009, "Development of Windows-based Program for Analysis and Visualization of Two-dimensional Stress Field in Digital Photoelasticity", *Songklanakarin Journal of Science and Technology*, Vol. 31, pp. 205-212.

8. Pinit, P. and Umezaki, E., 2007, "Digitally Whole-field Analysis of Isoclinic Parameter in Photoelasticity by Four-step Color Phase Shifting Technique", *Optics and Laser in Engineering*, Vol. 45, pp. 795-807.

9. Chang, C.W., Lien, H.S., and Lin, J.H., 2008, "Determination of Reflection Photoelasticity Fringes Analysis with Digital Image-Discrete Processing", *Measurement*, Vol. 41, pp. 862-869.

10. Chang, C.W., Chen, P.H., and Lien, H.S., 2009, "Separation of Photoelastic Principal Stresses by Analytical Evaluation and Digital Image Processing", *Journal of Mechanics*, Vol. 25, pp. 19-25.

11. Pinit, P., Nuttawat, P., and Saranyu, M., 2008, "A Simulation of Fringe Pattern of Stress Field for Photoelasticity", *Proceedings of the 6th PSU-Engineering Conference*, Songkla, Thailand, pp. 659-664. (In Thai)

12. Pinit, P., 2010, "Directions of Principal Stresses: Point-Wise and Full-field Analyses through a Problem in Theory of Elasticity", *Engineering Journal*, Vol. 2, pp. 1-20. (In Thai)

13. Pinit, P., 2009, "Flow of Stresses: Testing with a Simple Crack-based Technique", *Engineering Journal*, Vol. 1, pp. 26-40. (In Thai)

14. Kong, F.K. and Chemrouk, M., 2003, *Reinforced Concrete Deep Beams*, ed. Kong, F.K, Taylor & Francis, Glasgow and London.

15. Budynas, R.G. and Nisbett, J.K., 2008, *Shigley's Mechanical Engineering Design*, 8 ed. SI units, McGraw−Hill, New York.

16. Pinit, P., 2009, "Detection of Discontinuity in Map of Isoclinics in Digital Photoelasticity", *KMUTT Research and Development Journal*, Vol. 32, pp. 89-103. (In Thai)